

See discussions, stats, and author profiles for this publication at: <https://www.researchgate.net/publication/228110273>

# Quasi-Elastic Neutron Scattering Study of Translational Dynamics of Hydration Water in Tricalcium Silicate

ARTICLE *in* THE JOURNAL OF PHYSICAL CHEMISTRY B · JANUARY 2002

Impact Factor: 3.3 · DOI: 10.1021/jp010536m

CITATIONS

44

READS

36

## 4 AUTHORS:



**Emiliano Fratini**

University of Florence

123 PUBLICATIONS 2,371 CITATIONS

SEE PROFILE



**Sow-Hsin Chen**

Massachusetts Institute of Technology

469 PUBLICATIONS 15,588 CITATIONS

SEE PROFILE



**Piero Baglioni**

University of Florence

448 PUBLICATIONS 7,990 CITATIONS

SEE PROFILE



**M-C Bellissent-Funel**

French National Centre for Scientific Research

197 PUBLICATIONS 4,944 CITATIONS

SEE PROFILE

# Quasi-Elastic Neutron Scattering Study of Translational Dynamics of Hydration Water in Tricalcium Silicate

Emiliano Fratini,<sup>†,‡</sup> Sow-Hsin Chen,<sup>\*,†</sup> Piero Baglioni,<sup>‡</sup> and Marie-Claire Bellissent-Funel<sup>§</sup>

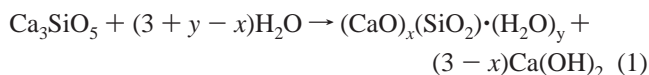
Department of Nuclear Engineering, 24-209, Massachusetts Institute of Technology, Cambridge, Massachusetts 02139, Department of Chemistry and CSGI, University of Florence, via G. Capponi 9, 50121 Florence, Italy, and Laboratoire Léon Brillouin (CEA-CNRS), CEA Saclay, 91191 Gif-sur-Yvette Cedex, France

Received: February 9, 2001; In Final Form: July 6, 2001

We investigate single-particle dynamics of water molecules in hydrated tricalcium silicate, a major component in ordinary Portland cement, as functions of temperature and aging and in the presence of an additive that retards the curing process. Spectra of incoherent quasi-elastic neutron scattering from hydrogen atoms were measured using a four-chopper spectrometer having an energy resolution of 28  $\mu\text{eV}$ , thus probing mainly the translational dynamics of water molecules. The spectra were analyzed with an explicit dynamical model. The model takes into account the existence of two types of water: “immobile water” (type one), presumably water bound inside colloidal particle component of the cement paste, and “glassy water” (type two), water imbedded in gellike component filling spaces between the colloidal particles. The model fits very well all normalized spectra in an absolute scale over a wide range of spectrum covering an energy transfer range of at least 300  $\mu\text{eV}$ . We deduced, from these fits, three important parameters as functions of temperature and aging and in the presence of an additive: (1) the  $Q$ -independent fraction of the immobile water ( $p$ ); (2) the  $Q$ -independent stretch exponent ( $\beta$ ), and (3) the  $Q$ -dependent average relaxation time ( $\bar{\tau}$ ) of the “glassy water”. From trends of the age dependence of these three parameters, we obtain a quantitative picture of the kinetics of the hydration process and the structural relaxation of the glassy water. We also conclude that there is no so-called “free” water in a cement paste (at least in the experimental conditions used in our experiments) at any time 1 h after its initial mixing with water.

## I. Introduction

Ordinary Portland cement (OPC) is a low-cost material for construction. Its composition is not fixed, but it varies according to the desired final application. Despite this, more than 50% (usually from 50% to 70% for most common applications) by weight of a OPC powder is constituted of tricalcium silicate so that  $\text{Ca}_3\text{SiO}_5$  is the simplest used model to study the hydration process characteristic of an ordinary cement paste.<sup>1</sup> When water is added to tricalcium silicate, nearly amorphous calcium hydrosilicate,  $(\text{CaO})_x(\text{SiO}_2) \cdot (\text{H}_2\text{O})_y$ , is formed by polymerization of monomeric silicate units, and this is accompanied by crystalline calcium hydroxide,  $\text{Ca}(\text{OH})_2$ , formation. The overall chemical reaction that takes place is schematized by<sup>2</sup>



where  $x$  represents the Ca-to-Si ratio in the calcium hydrosilicate gel (abbreviated as C–S–H<sup>3</sup>) and  $y$  is the sum of hydroxyl ions and bound water molecules incorporated into the gel structure. The two coefficients  $x$  and  $y$  change during reaction and throughout the sample and as function of the water/cement ratio and humidity conditions. While the real stoichiometry in

the C–S–H is still not clear and it is very difficult to obtain information about its nanometric structure due to its amorphous nature, it has been proven that the presence of the gel is the principal factor in the setting and hardening of the cement paste. Selected-area electron diffraction (SAED) and high-resolution electron microscopy (HREM) experiments<sup>4</sup> have shown that the mesostructure of cement paste consists of an amorphous matrix with a strongly variable composition which is embedded with nanocrystalline regions on the scale of  $\sim 50$  Å or less. Moreover, each nanocrystalline region has a locally homogeneous composition with short-range ordered regions on the scale of  $\sim 10$  Å with a variable composition and structure. On the other side, small-angle neutron scattering (SANS) experiments<sup>5</sup> have underlined the existence in the hydrated cement paste of a bimodal distribution of colloidal particles present just after mixing. The main component has a diameter of about 50 Å, while the size of second component appears to be about twice. These dimensions do not change during the time evolution of the curing process that only changes the volume fractal and the mass fractal dimensions<sup>6</sup> of the overall system. Previous NMR studies showed the presence of almost “solid-state” deuterated water, where the deuterium experience jumps of tetrahedral symmetry similar to those observed in  $\text{D}_2\text{O}$  ice between  $-6$  and  $0$  °C, and “liquid-state” water in rapid exchange with less mobile liquid water.<sup>7,8</sup> Similarly, quasi-elastic neutron scattering (QENS) experiments<sup>9,10</sup> have shown the presence of different type of water during the early stages of the curing process that can be described according to an Avrami and diffusion-limited kinetic models. A narrowing in the Lorentzian width in time

\* To whom all correspondence shall be addressed. Voice: (617) 253 3810. Fax: (617) 258 8863. E-mail: sowhsin@mit.edu.

<sup>†</sup> Massachusetts Institute of Technology.

<sup>‡</sup> University of Florence. E-mails: piero.baglioni@unifi.it and emiliano.fratini@unifi.it.

<sup>§</sup> Laboratoire Léon Brillouin (CEA-CNRS). E-mail: mcbel@llb.saclay.cea.fr.

has been noted,<sup>9</sup> but no detailed analysis of the relaxational dynamics of water has been reported in the paper. Moreover, an inelastic neutron-scattering (INS) experiment<sup>11</sup> has been used to monitor the growth of calcium hydroxide during the curing process. Combining this result, by previous QENS experiments, they have been able to extract the fraction of C–S–H in the paste as a function of time and temperature, confirming that<sup>12</sup> after 28 days the stoichiometric coefficient  $(3 - x)$  in eq 1 tends to 1.3 in the range of temperature 10–40 °C. According to the above picture of the microstructure of cured cement, the aggregated colloidal particles must be dispersed in some sort of interfacial water that contains calcium, hydroxide, and silicate ions. The diffusional dynamics of this interfacial water can be different from pure bulk water, depending on the concentrations of ions and structure of its gel matrix. Furthermore, motions of water molecules in the first and second hydration layers of the colloidal particles could be significantly retarded. As cement ages, water must penetrate more into the colloidal particles and became essentially immobile in the time scale of our experiment ( $2 \text{ ps} < t < 50 \text{ ps}$ ). Therefore, it is plausible to divide water molecules in a cement paste into two categories, according to their short time dynamics: a fraction  $p$  of immobile water molecules (bound water), and a fraction  $1 - p$  of less mobile water molecules. In this paper, we shall formulate the intermediate scattering function (ISF) of a water molecule explicitly according to the above picture. We shall show that the model accounts for the experimental spectra quite well and thus allows us to deduce the fraction  $p$  as a function of aging of the cement paste.

## II. Theoretical Background

Water is a triatomic and symmetric molecule consisting of two light hydrogen atoms and a heavier oxygen atom. Its center of mass is very nearly at the position of the oxygen atom. The incoherent neutron cross section of the individual hydrogen atom dominates the observed scattering cross section. Thus, as far as a QENS experiment of light water is concerned, we need only to consider motions of the individual hydrogen atom. Motions of the H-atom are composed of three components: vibrational motion of the atom around its equilibrium position; rotational motion of the atom around the center of mass; and the translational motion of the center of mass. It has been generally assumed in the literature that, for the purpose of calculating the QENS cross section, the intermediate scattering function (ISF) of the H-atom is a product of three factors each representing the time correlation function of the component motion. This simplification is called the “decoupling approximation”.<sup>13</sup> First of all, the equivalent time scale of observation of a typical QENS spectrum ( $1.0 \text{ ps} < t < 100 \text{ ps}$ ) is much longer than the vibrational period of the hydrogen atom. In this long-time limit, the vibrational ISF is effectively reduced to a Debye–Waller factor. For a high-resolution QENS experiment, the magnitude of the scattering wave vector  $\mathbf{Q}$  is always less than  $1.5 \text{ \AA}^{-1}$ . Since the equilibrium O–H bond is about  $1 \text{ \AA}$ , the vibrational amplitude of hydrogen atom around its equilibrium position cannot be larger than  $0.1 \text{ \AA}$ . Under this circumstance, the Debye–Waller factor is nearly unity for all  $\mathbf{Q}$  ranges of interest, and thus the vibrational contribution drops out of consideration. This means that for the purpose of analyzing a QENS spectrum, a water molecule can be treated effectively as a rigid molecule. The second issue, concerning us here, is the validity of the decoupling approximation. In a recent extensive computer molecular dynamics (MD) simulation of SPC/E model water (rigid molecules) at supercooled temperatures, Chen et

al.<sup>14</sup> showed that the decoupling approximation is good to a few percent for  $Q$  less than  $1 \text{ \AA}^{-1}$ , even though the rotational and translational motions of a water molecule are strongly coupled at all time. The most interesting point of observation from the MD simulation is that for time longer than about  $1 \text{ ps}$ , the ISF of the H-atom is closely approximated by that of the translational ISF. In the frequency domain, the dynamic structure factor calculated from the ISF of the H-atom is equal to that calculated from the translational ISF alone, plus a very small constant background coming from the convolution with the Fourier transform of the rotational ISF. This means that for all practical purpose, analysis of a high-resolution QENS spectrum needs only a theoretical expression for the translational ISF. This results in a great deal of simplification for the analysis of a QENS spectrum of  $\text{H}_2\text{O}$ .

A detailed discussion of the translational ISF for bulk water, which is an infinite medium, and its extension to the case of confined water has been given in reference.<sup>15</sup> For a translationally invariant system, the intermediate scattering function  $F_s(Q, t)$  can be derived from van Hove self-correlation function  $G_s(r, t)$  by a three-dimensional Fourier transform

$$F_s(Q, t) = \int e^{i\mathbf{Q} \cdot \mathbf{r}} G_s(r, t) d^3r \quad (2)$$

However, imposition of a confinement breaks the translational symmetry, and the van Hove self-correlation function is no longer a function of a scalar variable  $r$ . The self-correlation function  $G_s(\mathbf{r}, t | \mathbf{r}_0)$  now depends on both the test particle position  $\mathbf{r}$  at time  $t$  and its initial position  $\mathbf{r}_0$  at time zero. In this latter case, the intermediate scattering function has to be calculated according to a double integral

$$F_s(Q, t) = \int e^{i\mathbf{Q} \cdot (\mathbf{r} - \mathbf{r}_0)} G_s(\mathbf{r}, t | \mathbf{r}_0) p(\mathbf{r}_0) d^3r d^3r_0 \quad (3)$$

The intermediate scattering function is still a function of a scalar  $Q$  due to the orientational average one needs to make for an isotropic sample. In eq 3,  $p(\mathbf{r}_0)$  is the equilibrium distribution function of the test particle under the confining potential  $V(\mathbf{r})$ . It is easy to see that eq 3 reduces to eq 2 in the case of an infinite medium like a bulk liquid. In this special case,  $p(\mathbf{r}_0)$  is independent of the position and equals to an inverse of the sample volume.  $G_s(\mathbf{r}, t | \mathbf{r}_0)$  is now a function of  $|\mathbf{r} - \mathbf{r}_0|$  due to the translational symmetry. So the integration on the initial position can be carried out which cancels the volume factor.

Since the van Hove self-correlation function is a conditional probability of finding the test particle at  $\mathbf{r}$  at time  $t$ , given that the particle was at  $\mathbf{r}_0$  at time zero, there are three general properties the function has to satisfy. These in turn lead to three conditions for the ISF by its definition eq 3:

(i) normalization of the probability

$$\int G_s(\mathbf{r}, t | \mathbf{r}_0) p(\mathbf{r}_0) d^3r d^3r_0 = 1, \quad \text{leading to } F_s(Q=0, t) = 1 \quad (4)$$

(ii) the initial condition:

$$G_s(\mathbf{r}, t=0 | \mathbf{r}_0) = \delta(\mathbf{r} - \mathbf{r}_0), \quad \text{leading to } F_s(Q, t=0) = 0 \quad (5)$$

(iii) approach to a stationary distribution at sufficiently long time due to a confinement:

$$G_s(\mathbf{r}, t=\infty | \mathbf{r}_0) = p(\mathbf{r}) = \frac{1}{Z} \exp\left[-\frac{V(\mathbf{r})}{k_B T}\right],$$

leading to  $F_s(Q, t=\infty) = |\int e^{i\mathbf{Q} \cdot \mathbf{r}} p(\mathbf{r}) d^3r|^2 \quad (6)$

where  $Z$  is a normalization factor defined in such a way that the volume integral of  $p(\mathbf{r})$  for all space is unity. The  $Q$ -dependent factor,  $A(Q) = F_s(Q, t \rightarrow \infty)$ , is called the elastic incoherent structure factor (EISF) and is identical to the form factor of the confining volume. We shall discuss the following two examples which are relevant to the single particle dynamics in confined water.

(i) A water molecule bound at a location  $\bar{\mathbf{R}}$ . In this case,  $p(\bar{\mathbf{r}}) = \delta(\bar{\mathbf{r}} - \bar{\mathbf{R}})$ , and we have from eq 6

$$A(Q) = |e^{i\bar{\mathbf{Q}} \cdot \bar{\mathbf{R}}}|^2 = 1 \quad (7)$$

The corresponding ISF is  $F_s(Q, t) = 1$ . This result shows that if the test particle can be confined to a point  $\bar{\mathbf{R}}$  with a probability  $p$  but moving elsewhere with a probability  $1 - p$ , then the ISF can be written in a form

$$F_s(Q, t) = p + (1 - p)S(Q, t) \quad (8)$$

where the function  $S(Q, t)$  describes the motion of the test particle in the region where it is moving.

(ii) A water molecule confined inside a sphere of a radius  $a$ :

$$\text{EISF} = A(Q) = \left[ \frac{3j_1(Qa)}{Qa} \right]^2 \approx \exp\left(-\frac{1}{3}Q^2a^2\right) \quad (9)$$

Assuming that the test particle is diffusing inside the sphere, to a good approximation, the translational ISF can be put in the form:<sup>15</sup>

$$F_s(Q, t) = A(Q) + [1 - A(Q)]e^{-\Gamma(Q)t} \quad (10)$$

where line width  $\Gamma(Q)$  is related to the diffusion constants. The corresponding self-dynamic structure factor is

$$S_s(Q, \omega) = A(Q)\delta(\omega) + [1 - A(Q)]L(\omega, \Gamma) \quad (11)$$

$L(\omega, \Gamma)$  denotes a Lorentzian function of argument  $\omega$  and HWHM  $\Gamma$ . The spectral line shape for this case is a weighted superposition of an elastic peak and a quasi-elastic peak which is a Lorentzian in shape. Above examples form the basis of the following more realistic model.

### The Model

In this paper, we shall analyze the measured spectra according to the following model. We assume that at a given time there are two categories of water molecules in a cement paste: a fraction  $p$  of immobile water molecules bound inside the colloidal particles and a fraction  $1 - p$  of glassy water molecules imbedded in amorphous gel region surrounding the colloidal particles. According to the above assumptions, the ISF of the water in a cement paste can be written as

$$F_s(Q, t) = p + (1 - p)F_v(Q, t)e^{-(t/\tau)^\beta} \quad (12)$$

where the factor  $F_v(Q, t) \exp(-(t/\tau)^\beta)$  is the relaxation function of the glassy water according to a "relaxing cage model" previously given for supercooled water.<sup>16</sup> The model treats the short time dynamics of glassy water as vibrations of water molecules in an ensemble of harmonic wells arises from the cage effect, described by the factor

$$F_v(Q, t) = \exp\left\{-Q^2v_0^2\left[\frac{1-C}{\omega_1^2}(1 - e^{-\omega_1^2t/2}) + \frac{C}{\omega_2^2}(1 - e^{-\omega_2^2t/2})\right]\right\} \quad (13)$$

where  $\hbar\omega_1$  and  $\hbar\omega_2$  are the peak positions of the translational density of states of water<sup>13</sup> and  $C$  their relative strength. The long-time dynamics of cages is described by the " $\alpha$  relaxation" (the stretched exponential factor) follows from the "mode coupling theory".<sup>17,18</sup> This model was shown to fit an extensive set of ISF generated by computer molecular dynamics simulation of SPC/E<sup>19</sup> model supercooled water.<sup>20</sup> It was previously argued, with some experimental evidence, that the long-time dynamics of interfacial water behaves similarly to that of a bulk supercooled water at a lower temperature.<sup>21</sup> In this paper, we therefore use parameters  $\omega_1$ ,  $\omega_2$ , and  $C$  taken from the previous fits to MD data on supercooled water.<sup>16</sup>

### III. Experimental Section

**Samples.** The samples consist of about 1.5 g of dry  $\text{C}_3\text{S}$  powder (specific surface area 0.92  $\text{m}^2/\text{g}$  BLAINE, median diameter 6.7  $\mu\text{m}$ ), well mixed with about 1 g of bi-distilled water, to produce a paste with a 0.65 water/ $\text{C}_3\text{S}$  weight ratio. The paste so obtained was spread evenly into a rectangular aluminum cell making a layer of 0.5 mm thickness. The volume fraction of water in the sample was 0.60, making a film of  $\text{H}_2\text{O}$  of an effective thickness of 0.30 mm. The cell was reassembled and sealed by means of an indium wire gasket. This ensures a negligible loss of water as well as no contamination of the paste by carbon dioxide during the experiment. To prevent interference with the hydration process of the cement, the interior of the cell was coated by thin layer of Teflon to prevent contact of very basic paste with aluminum sample holder. Experiments were performed at two different temperatures: 15 and 30  $^\circ\text{C}$  averaging the signal every hour and following the kinetic for at least 1 day at each temperature. The experiment at 30  $^\circ\text{C}$  was repeated using an organophosphate retarder additive (1,5,9,13-tetra-aza-tridecane-1,1',5,9,13,13'-methylene-phosphonic acid,  $\text{C}_5\text{H}_{42}\text{N}_4\text{O}_{18}\text{P}_6$ , known commercially as Dequest 2086) solubilized in water to a concentration of 2000 ppm. The phosphonate molecules directly interact with the  $\text{C}_3\text{S}$  nuclei,<sup>22</sup> slowing down the growth process by increasing the induction period.

**Data Reduction and Fitting.** The quasi-elastic neutron scattering experiment was carried out at the Laboratoire Léon Brillouin (LLB) in Saclay, France, using a high-resolution time-of-flight (TOF) spectrometer MIBEMOL. The incident neutron wavelength was chosen at 9.0  $\text{\AA}$  (1.01 meV) to achieve a good energy resolution at the elastic peak position (fwhm about 28  $\mu\text{eV}$ ). The sample cell was placed at an angle making 45 $^\circ$  from the direction of the incident neutron beam in such a way that detector banks were in a reflection geometry. After scattering by the sample, neutrons are analyzed by 72  $^3\text{He}$  detector tubes as a function of time and angular position. To obtain an adequate statistics we grouped spectra from close-by detectors, excluding the Bragg peaks. The resulting  $Q$  range covered in our experiment was from 0.55 to 1.24  $\text{\AA}^{-1}$  having a set of five spectra resulting from the grouping. The transferred energy is measured by time-of-flight over 3.58 m of flight path of the scattered neutrons between the sample and detectors.

In an incoherent inelastic neutron scattering experiment of a water sample containing  $N/2$  molecules in the scattering volume, the measured scattered spectral intensity,  $I_s$ , per unit frequency

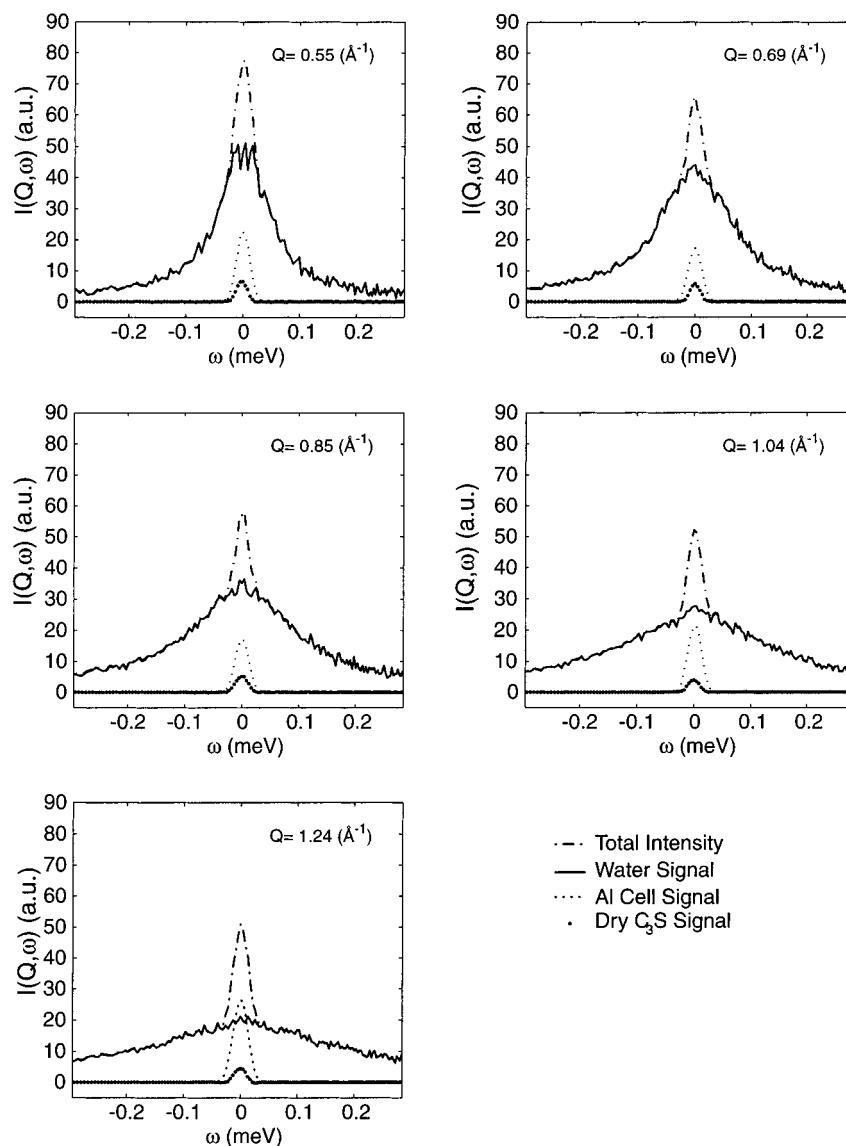


**Figure 1.** Components of a quasi-elastic neutron-scattering spectra for a sample hydrated for 1 h at 30 °C. The total intensity (dash-dot line) is composed of the water signal (solid line), the aluminum cell signal (dotted line), and the dry cement signal (filled circles).

interval and per unit solid angle subtended at the detector at a fixed distance from the sample is proportional to the incident neutron flux  $I_0$  times a double differential scattering cross section given by

$$\frac{\partial^2 \sigma}{\partial \omega \partial \Omega} = N \frac{\sigma_H}{4\pi} \frac{k}{k_0} S_s(Q, \omega) \quad (14)$$

where  $k_0$  is the wave vector of the monochromatic incident neutrons,  $k$  that of the scattered neutrons,  $Q$  the magnitude of the wave-vector transfer,  $\omega$  the energy transfer in the scattering process, and  $S_s(Q, \omega)$  the self-dynamic structure factor having a unit of seconds. The latter function has a property that its  $\omega$  integral from minus infinity to infinity is unity. The time-of-flight spectra, thus measured, were scaled by their monitor counts, corrected for scattering from the dry  $C_3S$  sample, converted in the energy space from the time channels space, and standardized by dividing by a scattering intensity from a thin vanadium plate. Due to a usual experimental limitation, slightly different orientations of the sample holders cannot be avoided. These small variations in sample orientations result in slightly different time channels for the elastic peak positions

for empty cell, vanadium, dry  $C_3S$  and  $C_3S$  paste. Such differences in the elastic peak position must be considered during the subtraction procedure. For this reason, the elastic position of the hydrated sample was fixed to  $E = 0 \mu\text{eV}$  and empty cell, vanadium and dry  $C_3S$  elastic peak positions were adjusted in such a way that all elastic peak positions coincided at the energy transfer scale  $E = 0 \mu\text{eV}$ . The measured spectral intensity normalized to unity is fitted by the following equation:

$$I_{\text{Water}}^M(Q, \omega) = S_s^{\text{Water}}(Q, \omega) \otimes R(\omega) \quad (15)$$

where  $R(\omega)$  represents the normalized vanadium spectral

$$S_s^{\text{Water}}(Q, \omega) = \text{FFT}[F_s(Q, t)] = p\delta(\omega) + (1 - p)\text{FFT}\{F_v(Q, t) \exp[-(t/\tau)^\beta]\} \quad (16)$$

intensity and the self-dynamic structure factor is the Fourier transform over the time space of the intermediate scattering function stated in eq 12. The fitting program used a Levenberg–Marquardt implementation of the nonlinear least squares problem;<sup>23</sup> standard methods were used to achieve the absolute errors on the fitting parameters<sup>24</sup>  $p$ ,  $\beta$ , and  $\tau$ .



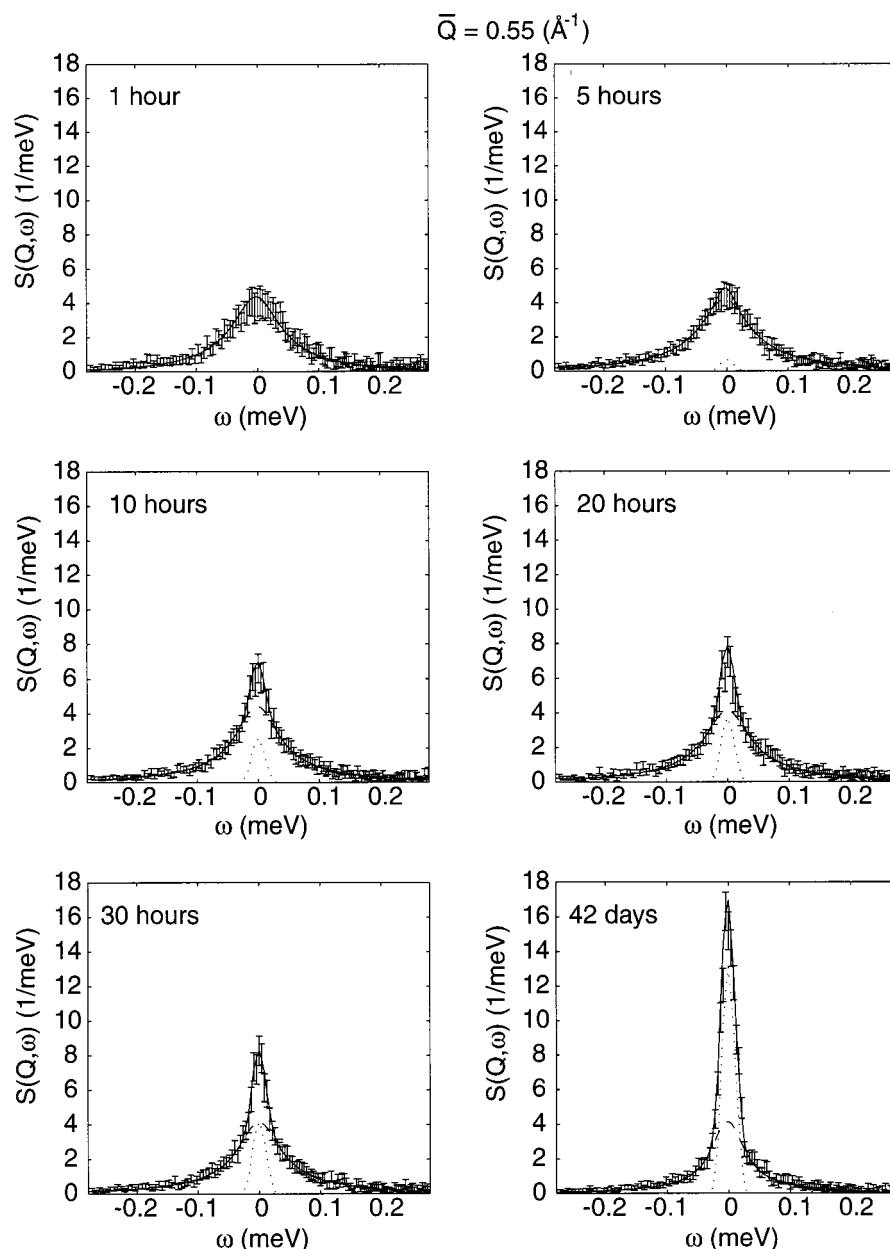


**Figure 2.** Time evolution of quasi-elastic incoherent neutron scattering spectra at  $\bar{Q} = 0.55 \pm 0.10 \text{ \AA}^{-1}$ . The points with error bars represent the normalized experimental spectra, solid lines are the fitted theoretical spectra, and thin solid lines and dotted lines are the quasi-elastic and elastic components (see eq 16), respectively, convoluted with the resolution function  $R(\omega)$ .

#### IV. Results and Discussion

The QENS spectra are constituted of several contributions coming out from the hydrogenated and non-hydrogenated components constituting the sample and from the empty cell. In the analysis of the data, the contribution from the non-hydrogenated components and from the empty cell have been subtracted from the QENS spectrum.

Figure 1 shows the different components constituting QENS spectra for the hydrated  $\text{C}_3\text{S}$  paste at each  $Q$  value considered. Just after the first hour, the components from hydrogenated species rule over signals from empty cell and from dry  $\text{C}_3\text{S}$ . While the water signal represents around 84% of the spectra, the dry  $\text{C}_3\text{S}$  is just the 1%, and the empty cell accounts for about around 15%. It is also evident that the quasi-elastic component comes only from the water fraction whereas empty cell and dry cement powder result in a pure elastic peak (as the vanadium used as reference). Therefore, the quasi-elastic peak component has a strong  $Q$  dependence, broadening with

increasing  $Q$ . Since we are interested in the translational dynamic of water, only the water component to the spectra will be treated in the following discussion.

The time evolution of the QENS spectra at  $\bar{Q} = 0.55 \text{ \AA}^{-1}$  and  $\bar{Q} = 1.04 \text{ \AA}^{-1}$  are reported in Figure 2 and Figure 3. The analysis of the spectra shows that (for both  $\bar{Q}$  and 1 h after the  $\text{C}_3\text{S}$  paste preparation) only a quasi-elastic component is present in the spectra. This contribution is non-Lorentzian with  $\beta = 0.79$  (see also Figure 6). The translational contribution to quasi-elastic scattering line-shape of bulk water at room temperature is typically Lorentzian<sup>13</sup> (i.e.,  $\beta = 1.0$ ) and usually in the literature is indicated as “free water”. A computer simulation of SPC/E model of water,<sup>20</sup> supercooled at 47 K below its maximum density temperature (4 °C), shows  $\beta = 0.75$ . Therefore, the water present in the cement paste (1 h after preparation) can be regarded as “glassy water” (see also below). Our data also show that, at least in the experimental conditions used in the present study, the amount of “free water” is

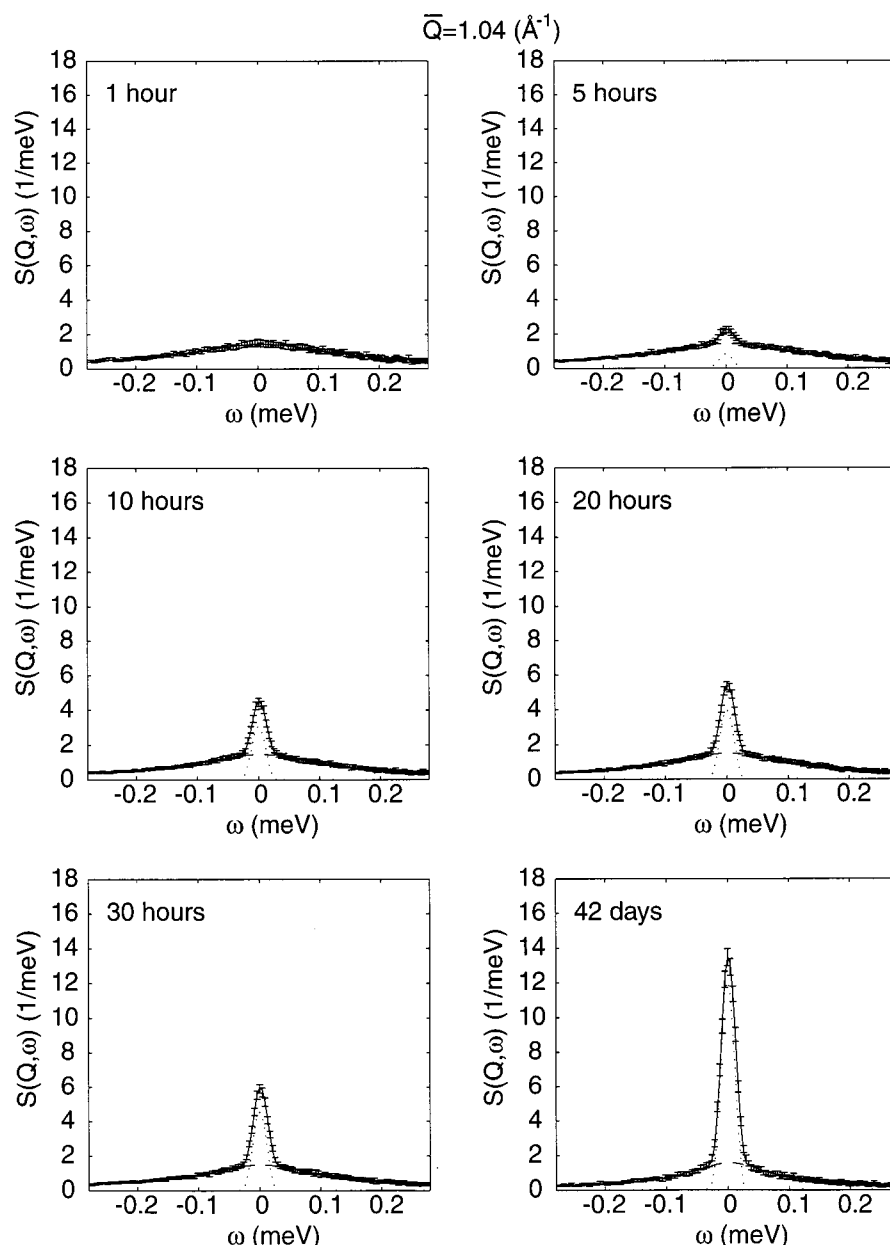


**Figure 3.** Time evolution of quasi-elastic incoherent neutron scattering spectra at  $\bar{Q} = 1.04 \pm 0.10 \text{ \AA}^{-1}$ . The points with error bars represent the normalized experimental spectra, solid lines are the fitted theoretical spectra, and thin solid lines and dotted lines are the quasi elastic and elastic components, respectively, convoluted with the resolution function  $R(\omega)$ .

negligible. An elastic contribution gradually increases as the cement paste ages, indicating that part of the “glassy water” is converted into immobile water. It is worthwhile to recall that some NMR studies<sup>8</sup> consider more than the two different kind of water used in our model for QENS analysis. Water mobility based on  $T_1$  and  $T_2$  relaxation times cannot be directly compared to the translational motion of water molecule detected by the QENS experiment, since NMR mainly detects dipolar interactions mostly associated to rotational motion. The de-coupling of rotational and translational motions is not trivial in a NMR experiment<sup>25</sup> particularly in a system subjected to a continuous change of chemical composition, as cement during the curing process.

During the hydration process, part of the water bounds into the calcium hydrosilicate (or calcium hydroxyde) formed during the chemical reaction. Since the total area of QENS spectra is normalized to the unity, it is possible to define a parameter  $p$ , that accounts for the fraction of water seen as immobile in the time scale accessible to QENS experiment ( $2 \text{ ps} < t < 50 \text{ ps}$ ).

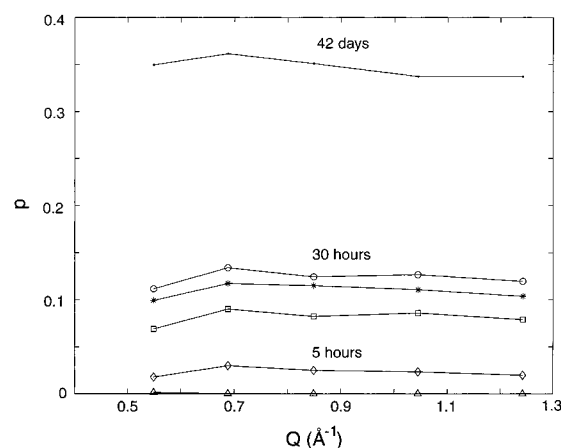


**Figure 4.** Dependence of  $p$  on the scattering vector  $Q = (4\pi/\lambda) \sin(\theta/2)$ , where  $\lambda = 9 \text{ \AA}$  and  $\theta$  is the scattering angle, after 1 h (triangles), 5 h (diamonds), 10 h (squares), 20 h (asterisks), 30 h (circles), and 42 days.

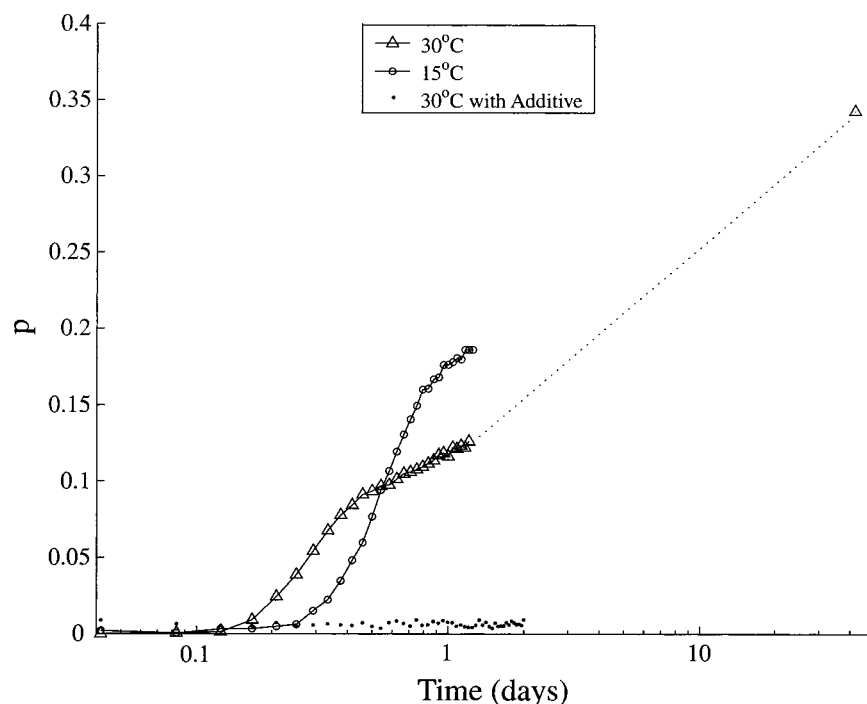


**Figure 5.** Time evolution of the fraction of immobile water at 30 (triangles), 15 (circles), and 30 °C with an additive (dots) that retards the curing process.

The  $p$  parameter can be easily determined from the area of the elastic peak, while the area fraction of the quasi-elastic component ( $1 - p$ ) gives directly the fraction of glassy water present in the cement paste. Therefore, this parameter provides direct information on the kinetic of the hydration reaction. Plots of the parameter  $p$  against the scattering vector  $Q$  at different times and for 30 °C (see Figure 4) indicate that this parameter is almost independent of the scattering vector, suggesting that “immobile” water molecules are highly localized (less than 1 Å) in the colloidal particles. Therefore, for each time of the curing process  $p$  is obtained as the average over five different scattering vectors  $Q$ .

Figure 5 reports the time evolution of the immobile water fraction at two different temperatures and in the presence of a commercial additive that retards the curing process. The analysis of the trend of  $p$  during the curing process clearly shows the presence of three different slopes in the plot  $p$  versus  $\log(t)$  and agrees with the three stage of a kinetic model already reported in the literature.<sup>1</sup> The kinetic model considers that in the curing cement are present: an induction period that lasts a few hours, an acceleration period that follows the classical random nucleation Avrami law<sup>26</sup> and a final stage controlled by a diffusion limited law. In our experiment,  $p$  increases only after an induction period. This induction period is, as expected, temperature-dependent and in particular is shorter for higher temperature. In this first reaction step, the water fraction converted from mobile to immobile is less at higher temperature because of the exothermal nature of the hydration process in the cement paste. The additive addition retards the conversion of glassy water to immobile water by more than 48 h, as shown by the invariance of  $p$  parameter in the period of time investigated (>48 h).

Additional information on the curing process can be obtained from the analysis of the  $\beta$  stretch exponent. Figure 6 shows that  $\beta$  decreases as a function of time. In analogy to the  $p$  parameter, the  $\beta$  exponent decrease at 15 °C is less pronounced than at 30 °C, and for both temperatures, the trend supports the presence of three stages in the hydration process. The  $\beta$  stretch

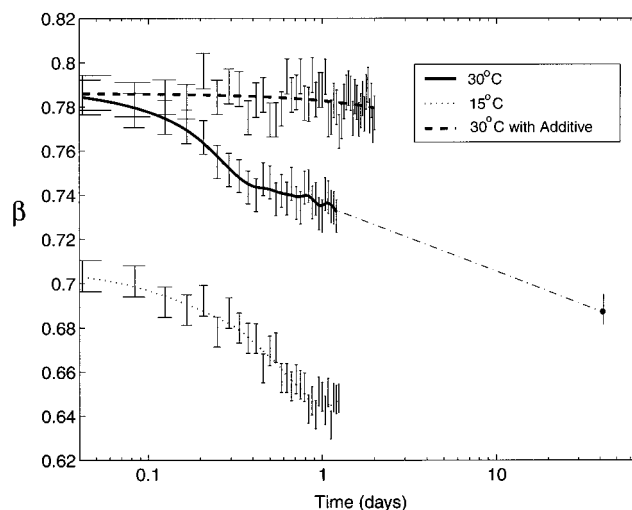


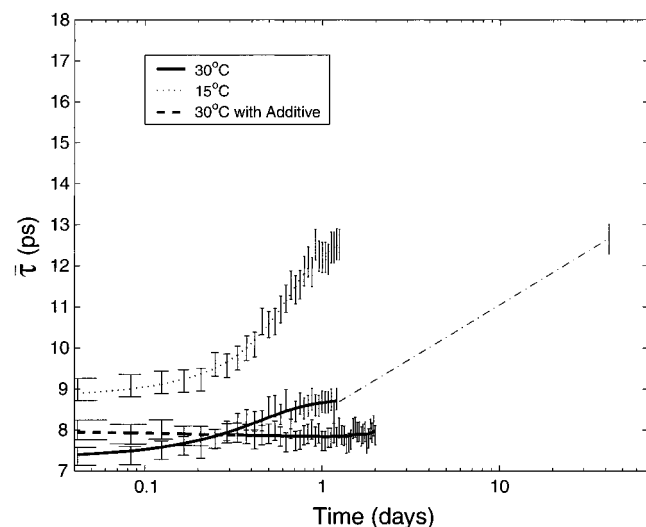
**Figure 6.** Time evolution of the stretch exponent  $\beta$  at 30 (solid line), 15 (dotted line), and 30 °C with an additive (dots) that retards the curing process.

exponent decrease indicates that the glassy water becomes “glassier” as time goes on, supporting an increase of water molecules’ confinement into the amorphous gel region. Moreover, the analysis of the  $\beta$  stretch exponent confirms that, in the presence of the additive, the glassy dynamics of water does not change during the time of the experimental investigation of the curing process.

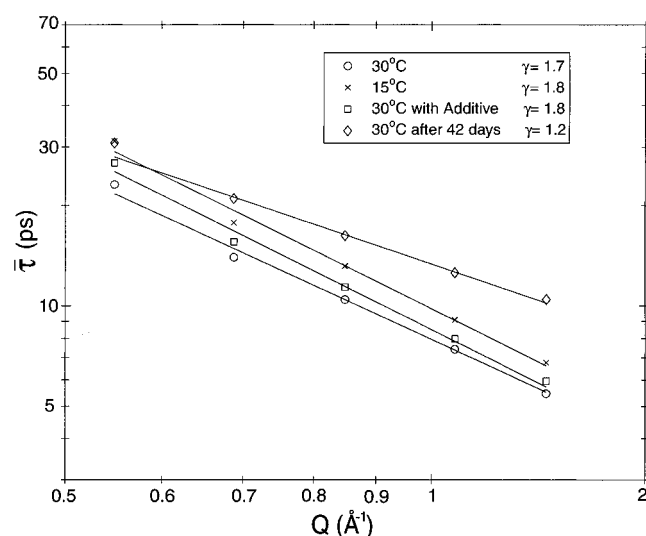
The increase of water confinement into the  $C_3S$  amorphous gel phase is also supported by the slowing down of the average structural relaxation time,  $\tau$ , as a function of time (see Figure 7).

Figure 8 clearly indicates that the average structural relaxation time has a power law dependence in  $Q$ , in agreement with previous finding of water confined in Vycor glasses<sup>27</sup> and with computer molecular dynamics experiments of bulk supercooled water.<sup>16</sup> It is observed that as far as the power-law exponent ( $\gamma$ ) is concerned, the aging of a cement paste has a similar effect





**Figure 7.** Time evolution of the average relaxation time,  $\bar{\tau} = (\tau/\beta)\Gamma(1/\beta)$ ,<sup>25</sup> at 30 (solid line), 15 (dotted line), and 30 °C with an additive (dashed line) that retards the curing process. Data obtained using the values at  $Q = 1.04 \pm 0.10 \text{ \AA}^{-1}$ .



**Figure 8.** Power law  $Q$ -dependence of  $\bar{\tau} \propto Q^{-\gamma}$ ,  $\gamma = 1.7 \pm 0.1$  for 30 °C (circle),  $\gamma = 1.8 \pm 0.1$  for 15 °C (crosses),  $\gamma = 1.8 \pm 0.1$  for 30 °C with the additive (square), and  $\gamma = 1.2 \pm 0.1$  for 30 °C after 42 days (diamonds).

as lowering the temperature in the case of a bulk supercooled water or water in Vycor. Again, the trend of the average structural relaxation time evidences three different kinetic steps and, in the presence of the retarding additive, the lacking of the water diffusional mobility modification.

## V. Conclusions

In this paper, we report for the first time a detailed analysis of quasi-elastic neutron scattering spectra in terms of the relaxational dynamics of water contained in a curing cement paste as a function of aging. The dynamical model proposed fits very well the entire set of the spectra collected over 42 days (more than 500 spectra), covering an energy transfer range of at least 300  $\mu\text{eV}$ . The model gives three important parameters: a  $Q$ -independent immobile water fraction ( $p$ ), the  $Q$ -independent stretch exponent ( $\beta$ ), and the  $Q$ -dependent average relaxation time ( $\tau$ ). These parameters have been deduced as a function of temperature and  $\text{C}_3\text{S}$  aging and in the presence of an additive that inhibits the curing process. The results clearly indicate, in

agreement with recent NMR results,<sup>7,8</sup> the presence of at least two different types of water in a curing cement paste, a “glassy water” and an “immobile water”. This latter water does not exhibit diffusional motion in the time scale of the QENS experiment ( $2 \text{ ps} < t < 50 \text{ ps}$ ). Free water is not detected just after 1 h from the beginning of the curing process, as demonstrated by the non-Lorentzian line shape of the quasi-elastic component of the QENS spectrum. The first type of water, defined as “glassy water”, similar in dynamic behavior to a supercooled bulk water, shows significant structural relaxation behavior and the Intermediate Scattering Function exhibits a slowly decaying component that can be accounted by the stretch exponent  $\beta < 1$ . The glassy water, present after 1 h from the beginning of the curing process, becomes “glassier” as indicated by the monotonic decrease of the stretch exponent  $\beta$  with the aging of the  $\text{C}_3\text{S}$  paste. We deduced, from the area of the elastic peak, the fraction of immobile water ( $p$ ), and the fraction of glassy water ( $1 - p$ ) as function of age. Thus, the curing process can be regarded as a continuous conversion of glassy water into immobile water. The analysis of the time evolution of  $p$  shows, as already reported in the literature, three different kinetic periods of the curing process. Moreover, these three periods can be also deduced from the slope change of the  $\beta$  versus time plot. The addition of the additive, inhibiting the curing process, is clearly detected by the  $\beta$  stretch exponent that does not change as a function of time. The model we proposed accounts for all the most important features of the curing process of cement paste. The  $\beta$  stretch exponent can be considered as the most important time-dependent parameter for the analysis of the curing process and its trend as a function of time (for very long period of time) would give information on both, the curing and the degradation process of cement.

**Acknowledgment.** Thanks are due to Dr. L. Cassar (CTG-Italcementi) for helpful discussion and for providing crystallographic pure  $\text{C}_3\text{S}$  sample. We are grateful to LLB of Saclay (France) for the use of the MIBEMOL spectrometer. The research of S.H.C. is supported by a grant from Material Research Program of US DOE. E.F. and P.B. acknowledge support from the Ministero Università Ricerca Scientifica e Tecnologica (MURST) and the Consorzio Sviluppo Sistemi a Grande Interfase (CSGI).

## References and Notes

- (1) Taylor, H. W. F. *Cement Chemistry*; Academic Press: London, 1990.
- (2) Tarrida, M.; Madon, M.; Rolland, B. L.; Colombet, P. *Adv. Cem. Based Mater.* **1995**, 2, 15–20.
- (3) In fact, in the widely accepted cement-chemistry notations  $\text{CaO}$ ,  $\text{SiO}_2$ , and  $\text{H}_2\text{O}$  become C, S, and H, respectively.
- (4) Xu, Z.; Viehland, D. *Phys. Rev. Lett.* **1996**, 77, 952–955.
- (5) Allen, A. J.; Oberthur, R. C.; Pearson, D.; Schofield, P.; Wilding, C. R. *Philos. Mag. B* **1987**, 56, 263–288.
- (6) Kriechbaum, M.; Degovics, G.; Tritthart, J.; Laggner P. *Prog. Colloid Polym. Sci.* **1989**, 79, 101–105.
- (7) Rakiewicz, E. F.; Benesi, A. J.; Grutzeck, M. W.; Kwan, S. *J. Am. Chem. Soc.* **1998**, 120, 6415–6416.
- (8) Greener, J.; Peemoeller, H.; Choi, C. H.; Holly, R.; Reardon, E. J.; Hansson, C. M.; Pintar, M. M. *J. Am. Ceram. Soc.* **2000**, 83, 623–627.
- (9) Fitzgerald, S. A.; Neumann, D. A.; Rush, J. J.; Bentz, D. P.; Livingston, R. A. *Chem. Mater.* **1998**, 10, 397–402.
- (10) Berliner, R.; Popovici, M.; Herwig, K. W.; Berliner, M.; Jennings, H. M.; Thomas, J. J. *Cem. Concr. Res.* **1998**, 28, 231–243.
- (11) Fitzgerald, S. A.; Neumann, D. A.; Rush, J. J.; Kirkpatrick, R. J.; Cong X.; Livingston, R. A. *J. Mater. Res.* **1999**, 14, 1160–1165.
- (12) Taylor, H. F. W.; Barret, P.; Brown, P. W.; Double, D. D.; Frohnsdorff, G.; Johansen, V. *Mater. Constr.* **1985**, 17, 457.
- (13) Chen, S. H. *Hydrogen-Bonded Liquids*; Kluwer Academic Publishers: Dordrecht, The Netherlands, 1991; pp 289–332.

- (14) Chen, S.-H.; Gallo, P.; Sciortino, F.; Tartaglia, P. *Phys. Rev. E* **1997**, *56*, 4231–4243.
- (15) Chen S. H.; Bellissent-Funel, M. C. *Hydrogen Bonded Networks*; Kluwer Academic Publishers: Dordrecht, The Netherlands 1994; pp 307–336.
- (16) Chen, S. H.; Liao, C.; Sciortino, F.; Gallo, P.; Tartaglia, P. *Phys. Rev. E* **1999**, *59*, 6708–6714.
- (17) Bengtzelius, U.; Gotze, W.; Sjolander, A. *J. Phys. C: Solid State Phys.* **1984**, *17*, 5915–5934.
- (18) Gotze, W.; Sjogren, L. *Rep. Prog. Phys.* **1992**, *55*, 241–376.
- (19) Berendsen, H. J. C.; Grigera, J. R.; Straatsma, T. P. *J. Phys. Chem.* **1987**, *91*, 6269–6271.
- (20) Sciortino, F.; Gallo, P.; Chen, S.-H.; Tartaglia, P. *Phys. Rev. E* **1996**, *54*, 6331–6343.
- (21) Chen, S. H.; Gallo, P.; Bellisset-Funel, M. C. *Can. J. Phys.* **1995**, *73*, 703–709.
- (22) Coveney, P. V.; Humphries, W. *J. Chem. Soc., Faraday Trans.* **1996**, *92*, 831–841.
- (23) Dennis, J. E., Jr. *State of Art in Numerical Analysis*; Academic Press; London, 1977; pp 269–312, and references therein.
- (24) Draper N. R.; Smith H. *Applied Regression Analysis*, 3rd ed.; Wiley: New York, 1981.
- (25) Magid, L. *Dynamic Light Scattering. The Methods and Some Applications*; Oxford University Press: Cambridge, 1993; pp 554–593.
- (26) Avrami, M. *J. Chem. Phys.* **1939**, *7*, 1103–1112.
- (27) Zanutti, J. M.; Bellissent-Funel, M. C.; Chen, S. H. *Phys. Rev. E* **1999**, *59*, 3084–3093.